How Bulk Nanobubbles Might Survive

Beng Hau Tan,[1,2] Hongjie An,[3,*] and Claus-Dieter Ohl[4,†]

[1]*School of Mechanical and Aerospace Engineering, Nanyang Technological University, 50 Nanyang Avenue, 639798 Singapore*
[2]*Low Energy Electronic Systems, Singapore-MIT Alliance for Research and Technology, 1 Create Way, 138602 Singapore*
[3]*Queensland Micro and Nanotechnology Centre, Griffith University, 170 Kessels Road, Nathan, Queensland 4111, Australia*
[4]*Otto von Guericke University Magdeburg, Institute of Experimental Physics, Universitätsplatz 2, 39016 Magdeburg, Germany*

(Received 3 July 2019; revised manuscript received 28 February 2020; accepted 3 March 2020; published 3 April 2020)

The existence of bulk nanobubbles has long been regarded with scepticism, due to the limitations of experimental techniques and the widespread assumption that spherical bubbles cannot achieve stable equilibrium. We develop a model for the stability of bulk nanobubbles based on the experimental observation that the zeta potential of spherical bubbles abruptly diverges from the planar value below 10 μm. Our calculations recover three persistently reported—but disputed—properties of bulk nanobubbles: that they stabilize at a typical radius of ~100 nm, that this radius is bounded below 1 μm, and that it increases with ionic concentration.

DOI: 10.1103/PhysRevLett.124.134503

Long lived, freely suspended and spherical nanoscopic bubbles, called nanobubbles [1–3], have been implicated in numerous unexplained phenomena, such as long lifetimes of positronium in liquid helium [4], or for the discrepancy in tensile strength of water between experiment and theory [5]. The last two decades has seen growing interest in nanobubbles for potential uses in water management [6,7], cleaning [8], medicine [9], and agriculture [10,11].

The diffusive dynamics of a spherical bubble in liquid is described by the Epstein-Plesset (EP) theory [12], which predicts the dynamics of spherical bubbles with radii as small as $R \sim 10$ μm with strong agreement to experiments [13,14]. However, it also predicts that bubbles experience either dissolution or unbounded growth, fueling long-standing scepticism over the existence of bulk nanobubbles ($R \sim 100$ nm).

Despite these objections, stable surface-attached nanobubbles [see Fig. 1(a)] have been proven to exist through numerous experimental techniques [15–19]. Stability is attributed to strong contact line pinning [20–22] compelling them to evolve in a constant footprint radius mode that permits regimes of stable equilibrium [23–26]. However, bulk nanobubbles cannot benefit from this mechanism, and thus remain controversial. Instead, it is variously proposed that bulk nanobubbles are stabilized due to a "skin" of contamination [27,28]; surface charges on the liquid-gas interface [29,30]; or substantially different surface tensions [31] or gas densities [32] from their macroscopic counterparts. None of these proposals have gained wide acceptance, however.

The experimental proof that bulk nanobubbles exist is also less than definitive. Dynamic light scattering (DLS) experiments [3] consistently claim that bulk nanobubbles have radii that (i) typically range from ~50 to 500 nm [8,34–36], (ii) appear to be strictly bounded to $\lesssim 1$ μm, and (iii) increase with ionic concentration [37–41]. However, sceptics do not regard DLS characterization as authoritative proof of the existence of bulk nanobubbles, since it depends on processing light-scattered speckle that cannot be unambiguously attributed to compressible bubbles. However,

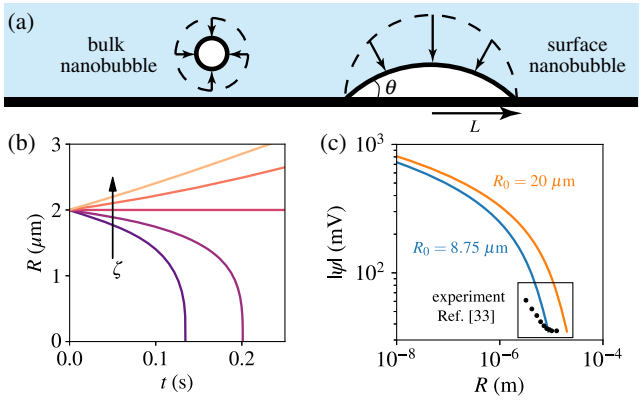

FIG. 1. (a) Schematics of a bulk and surface-attached nanobubble. As a bulk nanobubble shrinks, its radius decreases and the Laplace pressure driving dissolution accelerates. Conversely, in a shrinking surface nanobubble, the radius of curvature increases. (b) Direct solution of the EP model [Eqs. (1) and (2)] for a spherical bubble for [from bottom to top] oversaturations 0.8, 0.9, 1.0, 1.1, and $1.2\zeta_e$, where $\zeta_e = 2\gamma/R_0P_0$ is the equilibrium oversaturation of a bubble with radius $R_0 = 2$ μm. The bubble is static *only* at ζ_e; when $\zeta > \zeta_e$ it grows without bound, and when $\zeta < \zeta_e$ it dissolves into the solution. (c) Magnitude of zeta potential $|\psi|(R)$ of a shrinking bulk nanobubble of radius R under the assumption of charge conservation, as compared to the experiments of Takahashi, Chiba, and Li [33], for $R_0 = 8.75$ μm and $|\psi_0| = 35$ mV. For comparison a curve corresponding to $R_0 = 20$ μm is also shown.

these claims have been partially corroborated through electron microscopy of featureless voids in flash-frozen water [37,42], resonant mass [43], and refractive index measurements [39].

In this Letter we link the breakdown of zeta potential universality in shrinking spherical bubbles to the stability of bulk nanobubbles in aqueous solutions at equilibrium radii consistent with DLS experiments.

The EP model assumes that gas transport from the bubble obeys the diffusion equation, which in spherical geometry has the solution [12,44,45]

$$\frac{dR}{dt} = -\frac{D\Delta c}{\rho}\left(\frac{1}{R} + \frac{1}{\sqrt{\pi D t}}\right), \tag{1}$$

where D is the diffusion constant of dissolved gas in water, ρ is the density of gas, and $\Delta c = c_b - c_\infty$ is the concentration difference between the dissolved gas concentration c in the liquid adjacent to the bubble c_b and in the far-field c_∞. In all calculations we assign $D = 2 \times 10^{-9}$ m^2/s, $\rho = 1.165$ kg/m^3, and $c_s = 0.017$ kg/m^3. Substituting $c_b = P_b/k_H$ (where $P_b = P_0 + 2\gamma/R$ is the gas pressure in the bubble, γ is surface tension, and k_H is Henry's constant) yields

$$\Delta c = \left(P_0 + \frac{2\gamma}{R}\right)\frac{1}{k_H} - c_\infty = c_s\left(\frac{2\gamma}{RP_0} - \zeta\right), \tag{2}$$

where c_s is the saturation concentration, P_0 is atmospheric pressure, and we have defined [24] the oversaturation $\zeta = c_\infty/c_s - 1$, corresponding to $\zeta = 0$ for a gas-saturated liquid. As shown in Fig. 1(b), a spherical bubble grows without bound when $\zeta > \zeta_e$ [46], but dissolves completely when $\zeta < \zeta_e$. While a bubble is stationary at $\zeta_e = 2\gamma/R_0P_0$, environmental variations in ζ mean that, in practice, the bubble will observe only one of the first two outcomes.

A surface nanobubble avoids rapid dissolution due to contact line pinning [23–26], which compels it to maintain a fixed footprint radius L, see Fig. 1(a). This constraint *increases* its radius of curvature during shrinkage, thus reducing the Laplace pressure $\propto 1/R$ that drives dissolution [47]. The mathematical implication of line pinning is to reparametrize the dynamical equation from the form $\dot{R} = f(R)$ to $\dot{\theta} = f(\theta)$. Whereas the dynamical function $f(R)$ has one root (corresponding to an unstable equilibrium), the reparametrized $f(\theta)$ has two, the smaller of which is a stable equilibrium point [23,24].

These arguments suggest a path for the stabilization of bulk nanobubbles. If some physical effect modifies $\Delta c(R)$ [Eq. (2)] to have more than one root, stable equilibrium is assured, since in every pair of consecutive roots, one root crosses the R axis with a positive gradient, and the other with a negative gradient. (The equilibrium radius must also satisfy additional conditions, e.g., positive and submicron.) This principle explains the stability of particle-armored micro and nanobubbles (widely used as ultrasound contrast agents [48])—as a bubble shrinks, particles on the interface jam together, generating a growing mechanical stress in opposition to Laplace pressure [49].

We seek an analogous mechanism that applies to pure aqueous systems. It has been known since the 19th century [50] that water-gas interfaces are slightly negatively charged [33,51]. We therefore assume the freshly nucleated bubble holds an interfacial surface charge density $\sigma(R)$. The net charge exerts a mechanical pressure on the interface [52,53] given by $P_e = \sigma^2/2\epsilon\epsilon_0$, where ϵ_0 is the permittivity of free space, and the relative permittivity of water is $\epsilon \approx 80$ at 20 °C. Electrostatic stress on the surface acts radially outward, *regardless of the sign of the net charge*. By symmetry, repulsion between charges on a curved surface cancels everywhere except radially away from the bubble's center. Analogously, mechanical Laplace pressure arising from surface tension is directed towards the bubble's center, against electrostatic stress.

Surface charges on the bubble's liquid-gas interface draw charged particles in the liquid, assembling a diffuse double layer adjacent to the bubble's interface. For a monovalent spherical double layer of radius a, the surface charge density is given by

$$\sigma(a) = \frac{2\epsilon\epsilon_0\kappa k_B T}{e}\sinh\left(\frac{e\psi}{2k_BT}\right)f(a), \tag{3}$$

where $e = 1.6 \times 10^{-19}$ C is the elementary charge, k_B is the Boltzmann constant, T is temperature, ψ is zeta potential, $\kappa^{-1} = \sqrt{\epsilon\epsilon_0 k_B T/2c_0e^2}$ is the Debye length, c_0 is the ionic concentration, and

$$f(a) = \sqrt{1 + \frac{1}{\kappa a}\frac{2}{\cosh^2(\Psi/2)} + \frac{1}{(\kappa a)^2}\frac{8\ln[\cosh(\Psi/2)]}{\sinh^2(\Psi)}} \tag{4}$$

is a geometric term arising from an approximate solution to the spherical Poisson-Boltzmann equation derived by Ohshima *et al.* [54,55], where $\Psi \equiv e\psi/2k_BT$. In the large bubble limit $\kappa a \gg 1$, $f(a) \to 1$, and Eq. (3) becomes the Grahame equation for a planar double layer [56,57].

Bubbles larger than about 10 μm exhibit a universal zeta potential of about $\psi \approx -35$ mV, when measured by optical zeta potentiometry [58]. The equilibrium concentration of charge at the interface is specified by the chemical equilibrium between the interface and bulk. Since charged ions like hydroxide observe a potential-biased diffusion in the vicinity of the interface, equilibration is governed by the characteristic timescale $\tau \sim \ell^2/D \sim 10^{-11}$ s where $\ell \sim 1$ Å. This is substantially faster than the $\tau \sim R^2/D \sim 1$ ms shrinkage timescale of a 1 μm spherical bubble, and faster than the temporal resolution experimental techniques to measure zeta potential (~0.1 s for optical visualization and ~100 s for light scattering). Thus, one intuitively expects

the measured zeta potentials of spherical bubbles to be always at a constant value even if the charge distribution is perturbed.

Contradicting this expectation, Takahashi, Chiba, and Li [33] report that when a microbubble shrinks below about 8.75 μm, zeta potential universality abruptly breaks down, diverging from about $\psi = -35$ mV to about -60 mV at $R = 2.5$ μm. The breakdown of universality at the microscale is not fully understood, but there are several plausible reasons for its occurrence. The chemical equilibrium between the interface and bulk liquid—which determines the surface charge density—must be substantially different in a highly curved bubble as compared to a planar interface. For example, the curvature of the interface shifts the chemical potential of charged ions to be lower adjacent to a curved interface relative to a planar one [59]. This curvature correction becomes considerable at the microscale, allowing a curved interface to hold an elevated concentration of charge compared to a flat interface. Moreover, it is known from weak solution theory [60] that the presence of "trace solutes," e.g., ions or dissolved gas in the liquid solvent matrix, shift the chemical potential balance.

We do not aim to resolve the problem of what triggers breakdown of zeta potential universality but to focus on how the breakdown of universality influences the stability of bulk nanobubbles. To model this effect we consider to a first approximation that charge on the interface is conserved during shrinkage, $\sigma(R) = \sigma_0 R_0^2/R^2$, where σ_0 is the initial (i.e., at the point of the bubble's nucleation) surface charge density evaluated from Eqs. (3)–(4), and R_0 is the initial radius of the bubble at the point the accumulation begins. To show *a posteriori* that this is a reasonable assumption we compute the zeta potential accumulation implied by charge conservation by rewriting this balance as the transcendental equation $g(\psi) = \sigma_0(\psi_0, R_0)R_0^2 - \sigma(\psi, R)R^2$, using Eq. (3). Repeating this iteratively for $\psi_0 \approx -35$ mV and $R_0 \approx 8.75$ μm (both values extracted from Ref. [33]) for varying R thus yields $\psi(R)$, as shown in Fig. 1(c). An additional curve for $R_0 = 20$ μm is also plotted to provide an indication of sensitivity to initial conditions. Although the fitting is imperfect, this simple assumption reproduces—without adjustable parameters—the substantial accumulation of zeta potential reported by Takahashi *et al.* [33].

In the rest of this Letter, we examine the implications of the charge conservation assumption, which transforms Eq. (2) to

$$\Delta c = c_s \left[\frac{2\gamma}{RP_0} - \frac{2\epsilon\epsilon_0(\kappa k_B T)^2}{P_0 e^2} \sinh^2\Psi \cdot f^2(R_0) \frac{R_0^4}{R^4} - \zeta \right]. \quad (5)$$

Thus Eqs. (1) and (5) constitute our model. In practice R_0 is specific to the bubble generation technique. However, bubbles may also homogeneously nucleate in sufficiently oversaturated water. Treating water as a solvent containing trace quantities of dissolved gas [49,61], calculations [49] show that under typical conditions of $\zeta \sim 1$–2, one expects $R_0 \approx 2\gamma/P_0\zeta \sim 0.5$–$1.0$ μm.

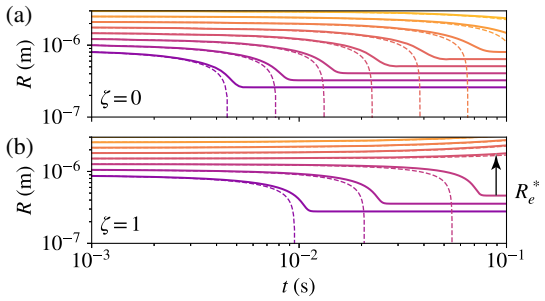

FIG. 2. Dynamical curves of spherical bubbles for oversaturations $\zeta = 0$ and $\zeta = 1$ under the assumption that they are stabilized by surface charges on the bubble [Eqs. (1) and (5), solid lines]. The Debye length $\kappa^{-1} = 10^{-8}$ m and initial zeta potential $\psi_0 = -30$ mV. The corresponding curves in the Epstein-Plesset model [Eqs. (1) and (2)] are overlaid in dashed lines. (a) When $\zeta = 0$, each bubble shown here is stable. (b) For finite oversaturation, here $\zeta = 1$, bubbles are stable for small R_0, but grow without bound beyond a threshold radius (here $R_0 \approx 1$ μm). The maximum equilibrium radius achieved before the transition to instability is R_e^*.

Let us now demonstrate how a spherical bubble that obeys charge conservation would evolve. In Figs. 2(a) and 2(b) we show a series of bubbles with initial radii $0.9 \lesssim R_0 \lesssim 3.0$ μm. We assume that the interfacial zeta potential before shrinkage commences is $\psi_0 = -30$ mV. Initially the shrinkage curves track the EP solution (dashed lines) closely, but later they abruptly stabilize. This effect originates from the rapid divergence of $P_e \sim 1/R^4$ [see Eq. (5)] relative to $P_L \sim 1/R$. Interestingly, the oversaturation ζ triggers a transition to instability. While all bubbles in Fig. 2(a) achieve a stable equilibrium at $\zeta = 0$, the corresponding ones for $\zeta = 1$ [Fig. 2(b)] stabilize only for $R_0 \lesssim 1$ μm, with larger bubbles growing without bound. When $\zeta \gtrsim P_e/P_0$, Eq. (5) approximates the EP solution [Eq. (2)], which is unstable [see Fig. 1(b)].

Next we explore the stable equilibrium radii R_e for the $\zeta = 0$ case; the finite oversaturation case is discussed later. Figure 3(a) shows how R_e depends on Debye length, for initial zeta potentials $\psi_0 = -5$, -10, -20, and -30 mV. Our key result is that spherical bubbles stabilize at the submicron scale in a wide spectrum of Debye lengths, namely from a strongly screened electrolyte to distilled water (1 Å $\lesssim \kappa^{-1} \lesssim 1$ μm). The dependence of R_e on κ^{-1}, however, shows contrasting behaviors at the spectrum's extremes. In the small κ^{-1} limit, i.e., large ionic strength, $R_e \propto \kappa^{2/3}$, which can be seen by noting $f(R_0) \to 1$ and seeking the root of Eq. (5). Conversely, for large κ^{-1}, $f(R_0) \propto 1/\kappa R_0$, eliminating the κ dependence in Eq. (5); thus, R_e becomes κ independent in solutions of low ionic strength.

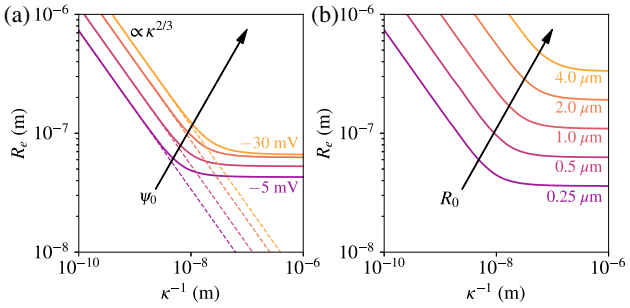

FIG. 3. Stable equilibrium radii R_e of bulk nanobubbles under the spectrum of Debye lengths of 1 Å $< \kappa^{-1} <$ 1 μm, for $\zeta = 0$. (a) Initial zeta potentials $\psi_0 = -5$, -10, -20, and -30 mV [from bottom to top] and $R_0 = 500$ nm. (b) Initial radii $R_0 = 0.25$, 0.5, 1.0, 2.0, and 4.0 μm [from bottom to top] and $\psi_0 = -20$ mV. The solid lines in (a),(b) denote solutions calculated from Ohshima's solution of the spherical Poisson-Boltzmann equation [Eq. (3)], while the dashed lines are the planar approximation, i.e., Grahame equation [Eq. (3) for $\kappa R_0 \gg 1$].

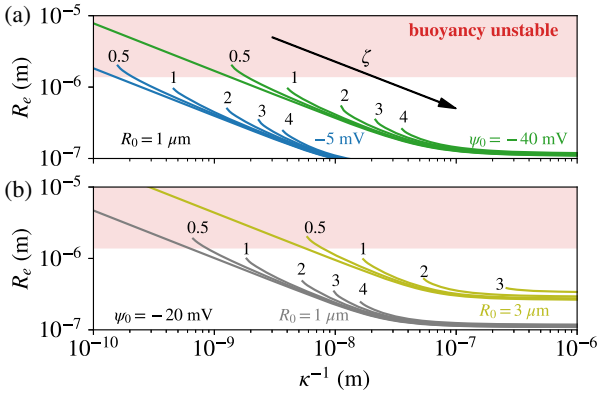

FIG. 4. Oversaturation and buoyancy influence size selection in bulk nanobubbles. The loci of stable equilibrium radii R_e as a function of Debye length κ^{-1}, for (a) fixed $R_0 = 1$ μm, and initial zeta potentials $\psi_0 = -5$ and -40 mV, and (b) fixed $\psi_0 = -20$ mV, and initial radii $R_0 = 1$ and 3 μm. These curves are calculated using Ohshima's equation [Eqs. (3) and (4)]. Unbroken lines correspond to the $\zeta = 0$ locus. As the oversaturation ζ increases from $0 < \zeta < 4$, bubbles establish a finite maximum equilibrium radius R_e^*, which decreases with increasing oversaturation. Buoyancy ensures that large bubbles overcome thermal energy and rise out of the bulk liquid at a threshold radius $R_b^* \sim \sqrt[4]{k_B T/\rho g} \sim 1$ μm, which is shaded pink.

These predictions compare well with DLS experiments that claim to produce bulk nanobubbles. Here we consider studies in which bubbles are nucleated and characterized in liquid of the same ionic strength (instead of generating the "nanobubbles" in distilled water before tuning the ionic concentration [34,35], possibly violating charge conservation). For a monovalent electrolyte at room temperature, a widely used empirical formula [56] states that $\kappa^{-1} \approx 0.304/\sqrt{I}$ nm, where I is the ionic strength in M (or mol L^{-1}). Objects thought to be bulk nanobubbles correspond to DLS peaks at $R_e = 80$, 100, and $\sim$1000 nm for 1 μM [39], 2 mM [8], and 1 M [39,62] solutions (corresponding to $\kappa^{-1} = 300$, 6.8, and 0.3 nm), respectively. Previously, it was speculated that the increase of R_e with ionic strength arises because electrolyte screening increases their propensity to coalesce into larger bubbles [41]. However, this hypothesis is not universally accepted, as Marangoni coarsening of the thin liquid film between approaching bubbles [63–65] could conversely discourage coalescence. Our model attributes the observed variation between R_e and κ^{-1} to the change in the electrocapillary stress balance in individual bubbles, instead of mutual interactions.

Finally, we offer an explanation for the observation in DLS experiments that bulk nanobubbles are almost always smaller than 1 μm. Size selection of spherical bubbles is achieved in two ways. First, finite oversaturation establishes a maximum possible equilibrium radius R_e^*. Figure 4 shows the loci of R_e in the parameter space of (κ^{-1}, R_e), varying $0 < \zeta < 4$. For $\zeta = 0$, the locus is uninterrupted, so bubbles always reach an equilibrium radius; but the finite oversaturation $\zeta > 0$ locus diverges from the $\zeta = 0$ locus and terminates at a maximum R_e^*. We show these loci in Fig. 4(a) for a fixed R_0 and $\psi_0 = -5$ and -40 mV, and in Fig. 4(b) for $\psi_0 = -20$ mV and $R_0 = 1$ and 3 μm. Oversaturation $\zeta > 0$ is required for nanobubbles to nucleate, through mechanical aeration of the water [10] or water-ethanol exchange [66,67], $\zeta \sim 1$–3 being generally reported. However, we also note that nanobubbles generated through external energy input in an environment without substantial oversaturation (e.g., by pressure variations [36,68] or electrochemistry [8]) can exist in stable equilibrium, too. Once nucleated, these bubbles are stable in exactly saturated ($\zeta = 0$) liquids.

Second, through buoyancy, all bubbles will rise through the liquid and leave the system [69], unless they are small enough that the work done by buoyancy $\sim \rho_l g R^4$ (where ρ_l is the liquid's density) is comparable to thermal energy $k_B T$. Balancing these terms yields a buoyancy threshold radius $R_b^* = \sqrt[4]{k_B T/\rho_l g} \approx 1$ μm ($g \approx 10$ m s^{-2} is the gravitational constant), above which a bubble is buoyancy unstable; this regime is shaded pink in Fig. 4. Once oversaturation establishes a size maximum and buoyancy removes all large bubbles, only submicron nanobubbles remain, consistent with the claims of DLS experiments that bulk nanobubbles have a maximum radius below approximately 1 μm [3,34].

In conclusion, our Letter rationalizes the stability of bulk nanobubbles in aqueous systems, in defiance of the "Laplace pressure bubble catastrophe" [3]—the seemingly inevitable fate of either dissolution or unbounded growth. Exploiting the experimental observation that the zeta potential of a shrinking microbubble abruptly deviates from its planar value below a radius of 10 μm, our model shows that bulk nanobubbles can potentially be stabilized by a mechanism of accumulating surface charge density.

While our results provide a theoretical basis for the viability of bulk nanobubbles, a definitive statement on their existence must be based on authoritative experimental validation, such as by coupling DLS with complementary techniques that probe the compressibility of suspended objects in liquid.

We acknowledge the support of the SMART Fellowship (to B. H. T.) and the Australian Research Council Future Fellowship (to H. A.). C. D. O. is supported by a joint research program between the Natural Science Foundation of China (Program No. 11861131005) and the Deutsche Forschungsgemeinschaft of Germany (Program No. OH 75/3-1).

Note added—We refer the reader to a recent dark-field microscopy study by Jin et al. [70], which reports that microbubbles shrink according to Epstein-Plesset dynamics before abruptly stabilizing at radii ∼100 nm.

*hongjie.an@griffith.edu.au
†claus-dieter.ohl@ovgu.de

[1] D. Lohse and X. Zhang, Rev. Mod. Phys. **87**, 981 (2015).
[2] J. R. T. Seddon and D. Lohse, J. Phys. Condens. Matter. **23**, 133001 (2011).
[3] M. Alheshibri, J. Qian, M. Jehannin, and V. S. J. Craig, Langmuir **32**, 11086 (2016).
[4] R. A. Ferrell, Phys. Rev. **108**, 167 (1957).
[5] K. A. Mørch, Phys. Fluids **19**, 072104 (2007).
[6] H. Zhang, T. Lyu, L. Bi, G. Tempero, D. P. Hamilton, and G. Pan, Sci. Total Environ. **637**, 550 (2018).
[7] L. Wang, X. Miao, J. Ali, T. Lyu, and G. Pan, ACS Omega **3**, 10624 (2018).
[8] J. Zhu, H. An, M. Alheshibri, L. Liu, P. M. J. Terpstra, G. Liu, and V. S. J. Craig, Langmuir **32**, 11203 (2016).
[9] A. Roy, K. K. Modi, S. Khasnavis, S. Ghosh, R. Watson, and K. Pahan, PLoS One **9**, e101883 (2014).
[10] K. Ebina, K. Shi, M. Hirao, J. Hashimoto, Y. Kawato, S. Kaneshiro, T. Morimoto, K. Koizumi, and H. Yoshikawa, PLoS One **8**, e65339 (2013).
[11] S. Liu, S. Oshita, S. Kawabata, and D. Q. Thuyet, Langmuir **33**, 12478 (2017).
[12] P. S. Epstein and M. S. Plesset, J. Chem. Phys. **18**, 1505 (1950).
[13] P. B. Duncan and D. Needham, Langmuir **20**, 2567 (2004).
[14] L. I. Berge, J. Colloid Interface Sci. **134**, 548 (1990).
[15] C. U. Chan and C.-D. Ohl, Phys. Rev. Lett. **109**, 174501 (2012).
[16] H. An, B. H. Tan, and C.-D. Ohl, Langmuir **32**, 12710 (2016).
[17] C. U. Chan, L. Chen, M. Arora, and C.-D. Ohl, Phys. Rev. Lett. **114**, 114505 (2015).
[18] X. Wang, B. Zhao, J. Hu, S. Wang, R. Tai, X. Gao, and L. Zhang, Phys. Chem. Chem. Phys. **19**, 1108 (2017).
[19] D. Seo, S. R. German, T. L. Mega, and W. A. Ducker, J. Phys. Chem. C **119**, 14262 (2015).
[20] X. Zhang, D. Y. C. Chan, D. Wang, and N. Maeda, Langmuir **29**, 1017 (2013).
[21] Y. Liu, J. Wang, X. Zhang, and W. Wang, J. Chem. Phys. **140**, 054705 (2014).
[22] B. H. Tan, H. An, and C.-D. Ohl, Phys. Rev. Lett. **118**, 054501 (2017).
[23] C. U. Chan, M. Arora, and C.-D. Ohl, Langmuir **31**, 7041 (2015).
[24] D. Lohse and X. Zhang, Phys. Rev. E **91**, 031003(R) (2015).
[25] B. H. Tan, H. An, and C.-D. Ohl, Phys. Rev. Lett. **120**, 164502 (2018).
[26] B. H. Tan, H. An, and C.-D. Ohl, Phys. Rev. Lett. **122**, 134502 (2019).
[27] F. E. Fox and K. F. Herzfeld, J. Acoust. Soc. Am. **26**, 984 (1954).
[28] K. Yasui, T. Tuziuti, W. Kanematsu, and K. Kato, Langmuir **32**, 11101 (2016).
[29] V. Akulichev, Acoust. Phys. **12**, 144 (1966).
[30] N. Bunkin and F. Bunkin, Sov. Phys. JETP **74**, 271 (1992).
[31] P. Attard, Eur. Phys. J. Special Topics **223**, 893 (2014).
[32] L. Zhang, H. Chen, Z. Li, H. Fang, and J. Hu, Sci. Chin. Ser. G: Phys. Mech. Astron. **51**, 219 (2008).
[33] M. Takahashi, K. Chiba, and P. Li, J. Phys. Chem. B **111**, 1343 (2007).
[34] N. Nirmalkar, A. Pacek, and M. Barigou, Langmuir **34**, 10964 (2018).
[35] N. Nirmalkar, A. Pacek, and M. Barigou, Soft Matter **14**, 9643 (2018).
[36] Z. Fang, L. Wang, X. Wang, L. Zhou, S. Wang, Z. Zou, R. Tai, L. Zhang, and J. Hu, J. Phys. Chem. C **122**, 22418 (2018).
[37] T. Uchida, S. Liu, M. Enari, S. Oshita, K. Yamazaki, and K. Gohara, Nanomater. Nanotechnol. **6**, 31 (2016).
[38] N. F. Bunkin, A. V. Shkirin, I. S. Burkhanov, L. L. Chaikov, and A. K. Lomkova, Quantum Electron. **44**, 1022 (2014).
[39] N. F. Bunkin, A. V. Shkirin, N. V. Suyazov, V. A. Babenko, A. A. Sychev, N. V. Penkov, K. N. Belosludtsev, and S. V. Gudkov, J. Phys. Chem. B **120**, 1291 (2016).
[40] F. Jin, X. Ye, and C. Wu, J. Phys. Chem. B **111**, 13143 (2007).
[41] F. Jin, J. Li, X. Ye, and C. Wu, J. Phys. Chem. B **111**, 11745 (2007).
[42] K. Ohgaki, N. Q. Khanh, Y. Joden, A. Tsuji, and T. Nakagawa, Chem. Eng. Sci. **65**, 1296 (2010).
[43] H. Kobayashi, S. Maeda, M. Kashiwa, and T. Fujita, in *International Conference on Optical Particle Characterization (OPC 2014)* (International Society for Optics and Photonics, Bellingham, 2014), Vol. 9232, p. 92320S.
[44] J. Crank, *The Mathematics of Diffusion* (Oxford University Press, Oxford, 1979).
[45] H. S. Carslaw and J. C. Jaeger, *Conduction of Heat in Solids* (Oxford University Press, Oxford, 1959).
[46] O. R. Enríquez, C. Sun, D. Lohse, A. Prosperetti, and D. van der Meer, J. Fluid Mech. **741** (2014).
[47] J. H. Weijs and D. Lohse, Phys. Rev. Lett. **110**, 054501 (2013).
[48] E. Stride and N. Saffari, Proc. Inst. Mech. Eng. H: J. Eng. Med. **217**, 429 (2003).
[49] N. Taccoen, F. Lequeux, D. Z. Gunes, and C. N. Baroud, Phys. Rev. X **6**, 011010 (2016).
[50] G. Quincke, Ann. Phys. (Berlin) **189**, 513 (1861).

[51] J. K. Beattie, A. M. Djerdjev, and G. G. Warr, Faraday Discuss. **141**, 31 (2009).
[52] E. M. Purcell and D. J. Morin, *Electricity and Magnetism* (Cambridge University Press, Cambridge, England, 2013).
[53] D. J. Griffiths, *Introduction to Electrodynamics* (Prentice Hall, New Jersey, 1999), 3rd ed.
[54] H. Ohshima, T. W. Healy, and L. R. White, J. Chem. Soc., Faraday Trans. 2 **79**, 1613 (1983).
[55] K. Makino and H. Ohshima, Langmuir **26**, 18016 (2010).
[56] J. N. Israelachvili, *Intermolecular and Surface Forces* (Academic Press, New York, 2011).
[57] H.-J. Butt and M. Kappl, *Surface and Interfacial Forces* (John Wiley & Sons, New York, 2018).
[58] M. Takahashi, J. Phys. Chem. B **109**, 21858 (2005).
[59] N. Kulkarni and R. Dehoff, Acta Mater. **45**, 4963 (1997).
[60] L. D. Landau and E. M. Lifshitz, *Statistical Physics, Third Edition, Part 1: Volume 5*, 3rd ed. (Butterworth-Heinemann, Amsterdam, 1980).
[61] C. Ward, A. Balakrishnan, and F. Hooper, J. Basic Eng. **92**, 695 (1970).
[62] N. Bunkin, A. Shkirin, P. Ignatiev, L. Chaikov, I. Burkhanov, and A. Starosvetskij, J. Chem. Phys. **137**, 054706 (2012).
[63] H. Christenson and V. Yaminsky, J. Phys. Chem. **99**, 10420 (1995).
[64] P. K. Weissenborn and R. J. Pugh, J. Colloid Interface Sci. **184**, 550 (1996).
[65] V. S. J. Craig, Curr. Opin. Colloid Interface Sci. **9**, 178 (2004).
[66] J. C. Millare and B. A. Basilia, ChemistrySelect **3**, 9268 (2018).
[67] M. Alheshibri and V. S. Craig, J. Colloid Interface Sci. **542**, 136 (2019).
[68] Q. Wang, H. Zhao, N. Qi, Y. Qin, X. Zhang, and Y. Li, Sci. Rep. **9**, 1118 (2019).
[69] L. Parkinson, R. Sedev, D. Fornasiero, and J. Ralston, J. Colloid Interface Sci. **322**, 168 (2008).
[70] J. Jin, R. Wang, J. Tang, L. Yang, Z. Feng, C. Xu, F. Yang, N. Gu, Colloids Surf. A **589**, 124430 (2020).